Fission fragment atomic number measurements using Bragg detectors

Sosnin, N.V.; Smith, A.G.; Wright, T.; Köster, U.; Blanc, A.; Nara Singh, B.S.; Kennedy-Reid, R.L.; Davies, P.J.

Published in:
Nuclear Instruments and Methods in Physics Research Section A: Accelerators, Spectrometers, Detectors and Associated Equipment

DOI:
10.1016/j.nima.2020.163397

Published: 21/03/2020

Document Version
Publisher's PDF, also known as Version of record

Nuclear Inst. and Methods in Physics Research, A 957 (2020) 163397

Contents lists available at ScienceDirect

Nuclear Inst. and Methods in Physics Research, A

journal homepage: www.elsevier.com/locate/nima

Fission fragment atomic number measurements using Bragg detectors

N.V. Sosnin [a,*], A.G. Smith [a], T. Wright [a], U. Köster [b], A. Blanc [b], B.S. Nara Singh [a,c], R.L. Kennedy-Reid [a], P.J. Davies [a]

[a] Schuster Laboratory, The University of Manchester, Manchester, M13 9PL, UK
[b] Institut Laue-Langevin, Grenoble, France
[c] School of Computing, Engineering and Physical Sciences, University of the West of Scotland, Paisley, PA1 2BE, UK

ARTICLE INFO

Keywords:
Fission fragment charge
SRIM
Ionization chamber
Sub-Bragg peak spectroscopy
Lohengrin
Fission fragment range

ABSTRACT

A Bragg detector with a Frisch grid and 1 metre-long time-of-flight section with microchannel plate assemblies was characterized at the Lohengrin fission fragment separator at the Institut Laue-Langevin (ILL) by measuring ^{235}U fission fragments of selected masses and energies at the Lohengrin focal plane. The aim of the measurements was to investigate the response of Bragg detectors to differing nuclear charge states. Energy-loss and a signal-risetime dependent parameters were defined and extracted from the accumulated signal pulse shapes, and their behaviour as a function of fragment velocity was investigated. The experimental results are compared to a SRIM-2013 simulation. Measurements of fission fragment ranges in isobutane are presented. Average proton numbers for measured fragment masses were identified and could be resolved by the parameters, which exhibited monotonic variation with charge. The results differed from SRIM both in trends and in values, with SRIM simulations exhibiting non-monotonic behaviour with proton number.

1. Introduction

Interaction of ions in matter has been a field of great interest throughout the history of physics, critical to many significant discoveries, for example the discovery of atomic structure resulting from the Geiger–Marsden experiment [1]. The stopping in matter of fast ions travelling at velocities $v \gg v_0$, where v_0 is the Bohr velocity equal to 2.19×10^6 m/s, is relatively well-understood. The differential energy loss of these ions in gaseous media, such as in a Bragg detector (BD), can be described with the Bethe–Bloch formula, which gives the stopping power $S(E)$ based on ion velocity and charge. Experimental methods for extracting proton number Z information from the energy loss maximum, i.e. the Bragg peak, have been proposed by Gruhn et al. [2] and used extensively in many nuclear physics experiments and applications [3–6]. Ion velocities below or around the Bohr velocity may be insufficient to fully ionize the atom [7], resulting in electronic screening of the nuclear charge and possible electron exchange with the gas. Subsequent variation of the effective charge of the ion prevents a Bragg peak from forming in the energy loss profile. This is the case for fission fragments (FF), which typically have velocities of the same order of magnitude as the Bohr velocity. Comparative examples of energy loss profiles simulated in SRIM-2013 [8] for typical light fragments are shown in Fig. 1. All the fragments in the figure have kinetic energy-to-mass ratios of 1 MeV/amu. Panel (a) shows the effect of increasing range with increase in mass for three krypton isotopes. FFs are produced with a large range of masses and atomic numbers, and panel (b) of Fig. 1 demonstrates the difficulty in distinguishing energy loss profiles of three typical ^{235}U fragments, $^{90}_{36}$Kr, $^{95}_{38}$Sr and $^{100}_{40}$Zr.

The nuclear charge yields of FF are required to understand the fission process and for a multitude of applications, therefore a variety of methods have been developed to measure these independent charge yields, that is nuclear charge before FF undergo radioactive decay. For unaccelerated FF, such methods frequently involve the use of γ- or X-ray spectroscopy [9–11], but these techniques result in yields that depend on knowledge of the level schemes. Alternatively, ΔE-E telescopes can be used [12–14]. Such telescopes rely on energy loss similarly to Bragg peak spectroscopy, however ΔE-E telescopes are typically limited by their charge resolution and can only measure charge yields in the light fragment group up to $Z \approx 42$ [15], and up to $Z \approx 52$ [16] if a calorimetric low-temperature detector is used.

Since fission is a result of competition between electrostatic and nuclear force, the information on the charge distribution is critical in understanding the dynamics of a nucleus undergoing fission, as well as informing models of the fission process [10,17]. Charge yields have significant implications for nuclear energy applications, where they have direct application to nuclear waste composition [18], reactor heating [19], as well as providing input towards addressing the reactor antineutrino anomaly [20]. Furthermore, measurements of FF in correlation with neutrons [21,22] and gamma rays [23,24] produced

* Corresponding author.
E-mail address: nikolay.sosnin@manchester.ac.uk (N.V. Sosnin).

https://doi.org/10.1016/j.nima.2020.163397
Received 20 September 2019; Received in revised form 13 December 2019; Accepted 3 January 2020
Available online 10 January 2020
0168-9002/

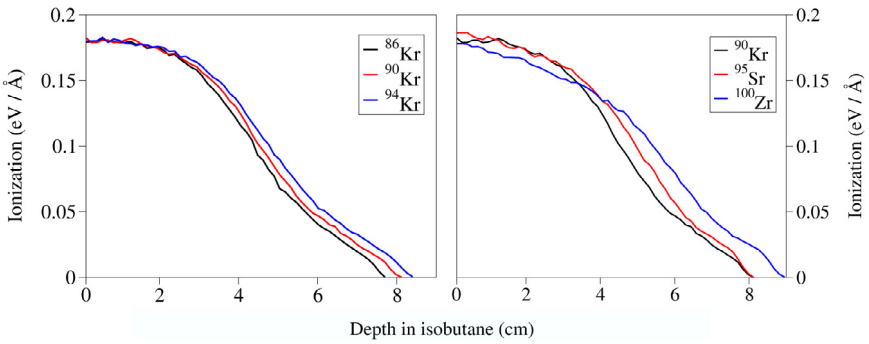

Fig. 1. Profiles of simulated average energy loss with range in 100 mbar of isobutane by fragments with kinetic energy-to-mass ratios of 1 MeV/amu. Panel (a) shows energy loss by ^{86,90,94}Kr fragments illustrating the effect mass has on stopping. Panel (b) shows ^{90}Kr, ^{95}Sr and ^{100}Zr energy loss, demonstrating differences in energy loss with change in atomic number and mass for typical ^{235}U fission fragments. The profiles were simulated and averaged over 20 fragments of each type using SRIM-2013.

in fission have been a subject of continued interest. Large detector assemblies, such as the SpecTrometer for Exotic Fission Fragments (STEFF) [25], use BDs to provide FF information. Developing a methodology for extracting proton number information from the BD signals would greatly benefit the potential of such spectrometers and the data provided for fission models. In order to develop such a methodology, a BD-based spectrometer called Fission Fragment Identification (FiFI) arm was constructed at the University of Manchester, UK, and used in an experimental campaign measuring FF from thermal neutron induced fission of ^{235}U at ILL, using the constant velocity FF beam provided by the Lohengrin facility. BD digitized waveforms for various Lohengrin settings were stored and analysed in an effort to construct a functional form that can be used for calibrating BDs and extracting the FF Z using differential energy loss and range. Examining the FF stopping process using pulse shape analysis of stored waveforms allows for an investigation of the details of the stopping without reliance on prominent features such as the Bragg peak.

2. Fission fragment identification arm

FiFI is composed of two sections: a time-of-flight (ToF) section and a BD. A diagram of the setup is presented in Fig. 2. The ToF section, located between volumes B and C, relies on two timing detectors separated by a 1-metre flightpath. The START and STOP timing detectors, positioned in volumes B and C, are identical microchannel plate (MCP) assemblies. The assemblies feature thin foils marked D, an electrostatic mirror, marked E, and a MCP denoted with F. The foils are made of $\approx$ 0.3μm formvar, coated in 370 Å aluminium. The foils are circular with a diameter of 8 cm, deposited on a steel grid of thin wires (0.2 mm diameter) with a 1 cm × 1 cm square lattice and a transparency of ≈96%. When FF pass through the foil, some of the electrons ejected from the foil may be backscattered. The backscattered electrons are redirected upwards by an electrostatic mirror, which is a grid of 20-micron thick wires held at a potential of 4 kV, and has a transparency of ≈97.2%. The electron current is then multiplied by Hamamatsu F1942-04 MCPs [26] held at 2 kV potential. The resulting timing resolution of the ToF section of FiFI is 1.2 ± 0.1 ns measured using alpha particles. For the data presented in this work, the ToF section of the device was not used and its foils were removed in order to avoid FF straggling.

The BD on FiFI is a cylindrical volume containing 12 field-shaping rings, a Frisch grid and an anode. The chamber is filled with 100 mbar of isobutane gas and is isolated from the vacuum of the ToF section using a 0.5 μm Mylar window covered with a steel collimator, denoted with letter G in Fig. 2. The collimator contains a thin rectangular slit that is 4 cm long and 0.8 cm wide. The BD anode (located at position H in Fig. 2) is held at a potential of 1.4 kV, the Frisch grid at 1.2 kV and the field-shaping rings are held at potential increments of 100 V. The grid and the anode (and all the field-shaping rings) are separated by 1 cm spacers. The Frisch grid comprises a series of parallel 20 μm thick wires at a separation of 2 mm. Frisch grid and anode signals are routed through Cooknell EC572 charge sensitive preamplifiers and full signal traces were recorded using CAEN V1724 ADCs. For 80 MeV incident FF, the energy resolution of the BD is ≈500 keV.

3. FiFI at Lohengrin

In order to establish the response of the BD, a source of FF with known charge states was necessary. The Lohengrin separator [27] is a unique device, which can provide intense beams of selected fragments with an excellent mass and energy resolution. Fragments are produced by fission taking place in a thin layer of fissile material (^{235}U in the case of this work) exposed to a neutron flux of 5×10^{14} cm^{-2}s^{-1} inside the high-flux reactor at ILL. Neutron-induced fission fragments recoil from the target layer with their kinetic energy obtained in the fission process, and, due to electron stripping in the layer and its 0.25 μm nickel cover foil, emerge as highly ionized (typical q from 17 to 26) ions. These ions travel through the Lohengrin beamline, where a dipole magnet and electric condenser field act to select a beam of FF based on their A/q and E/q ratios. Here A is the mass of the fragment, E is the kinetic energy, and q is the ionic charge. FF time of flight through Lohengrin is ≈2 μs [27], a time that is shorter than fragment β half lives, meaning that Lohengrin beams at the focal plane comprise only FF that have undergone prompt neutron emission, and not β^- decays or delayed neutron emission. The fragments selected by Lohengrin arrive at the focal plane with a known velocity and separated by mass/energy. Since FF are emitted with different ionic charges, the beam at the focal plane will contain FF with a number of different mass and energy combinations. Moreover, each FF mass setting will contain several isobars. Nonetheless, for typical Lohengrin beam settings the separation between adjacent selected mass or energy FFs can be easily resolved by the BD. More importantly, the combination of known velocity and a variety of Z states of the Lohengrin beams makes Lohengrin ideal for testing the stopping power dependence on Z.

FiFI was installed at the focal plane of Lohengrin and operated for 14 days, collecting ionization traces from 60 different Lohengrin setting combinations, where the timing foils were removed to prevent FF straggling. Amongst the 60 setting combinations, some were in the symmetry region and are not used in the analysis here due to poor statistics, which reduces the number of settings combinations ultimately used to 40.

Several digital filters have been applied to the anode waveforms. A combination of differentiator and infinite integrator filters was used to zero the baseline and remove low-frequency noise, and a low-pass 6-pole Chebyshev filter was used to filter out high-frequency noise. A ballistic deficit correction was applied during the extraction of maximal energy loss to compensate for the decay time of the charge-sensitive preamplifier. A Moving Window Deconvolution filter [28] was used for extracting the maximal amplitude of the pulses. Lastly, a Frisch

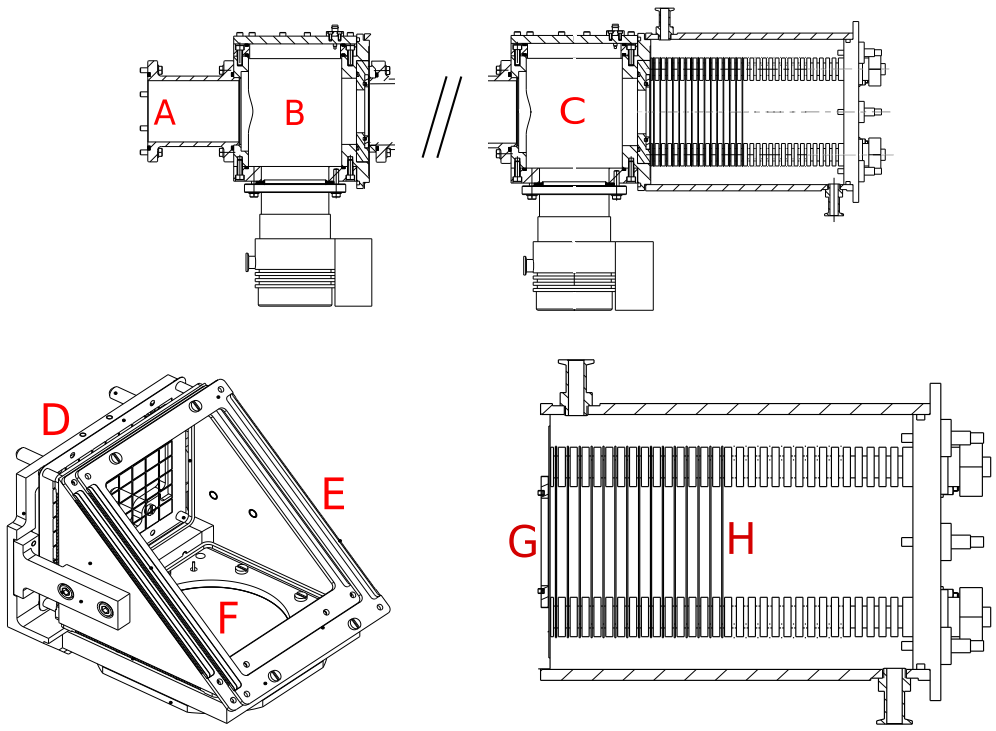

Fig. 2. A schematic diagram of the Fission Fragment Identification arm. The entry point of a FF beam is marked with letter A. Letters B and C denote volumes where the START and STOP detector assemblies are positioned. The positions of the vacuum pumps are shown beneath those volumes. The 1 metre-long ToF section has been truncated for the purposes of the diagram. An expanded view of the timing detectors is shown in the bottom left part of the diagram. Letter D marks the location where the mesh supporting the emission foil is located. Letter E denotes the plane onto which the electrostatic mirror is attached. The MCP is located at letter F. Note that the timing detector in the diagram is shown upside down compared to its actual orientation inside FiFI. An expanded view of the BD is shown in the bottom right corner. The mylar window is at letter G, followed by a gas-filled volume containing the field-shaping rings, the Frisch grid and an anode (position H). ToF foils were removed during data collection for the results presented in this work.

grid inefficiency correction has been applied to the anode signal in accordance with the method of Göök *et al* [29]. The grid inefficiency was found to be 8.8%.

The FF energy was taken as the maximum amplitude of the corrected anode signals and a resulting typical spectrum is shown in Fig. 3 for Lohengrin settings of $A = 80$ amu, $q = 20$ and $E = 80$ MeV. Using such energy spectra, matrices were constructed of FF energy against average signal shape. Such matrices allowed gating on mass peaks, such as the ones in Fig. 3, to produce average FF waveforms for various single masses and energies, but containing contributions from several isobars. A typical gated waveform was averaged over 8000 FF. The averaged pulse shapes and their derivatives were used to extract three parameters: Q_{max}, which corresponds to the anode signal maximum, ${}^{dQ}/_{dt}|_{max}$, which is a maximum anode current related to maximal energy loss, and t_{10-90}, which is the 10% to 90% risetime of the anode signal. These parameters correspond to the fragment energy, maximum energy-loss, and range respectively. A typical anode signal with its derivative is shown in Fig. 4.

The parameters extracted from the pulses have been used to examine the pulse shape dependence on fragment Z. The energy and energy-loss parameters have been combined in a ratio ϵ defined as

$$\epsilon = \frac{{}^{dQ}/_{dt}|_{max}}{Q_{max}}, \tag{1}$$

where division by Q_{max} serves to reduce systematic errors due to gain of the anode over the experimental campaign, since Q_{max} and ${}^{dQ}/_{dt}|_{max}$ will both be affected by any drift in the anode gain in similar ways. This parameter depends on Z, A and v, hence in order to remove the mass dependence, the Lohengrin mass setting is used to produce the final parameter

$$A\left(\frac{v}{c}\right)^2 \epsilon. \tag{2}$$

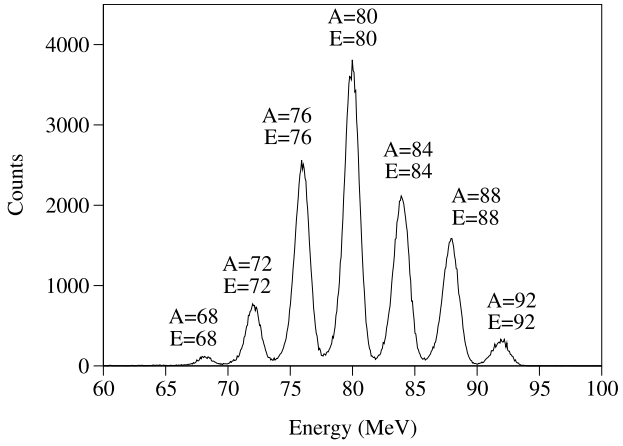

Fig. 3. A typical energy spectrum extracted from the filtered and corrected anode signals for Lohengrin settings $A = 80$ amu, $q = 20$, $E = 80$ MeV. The peaks in the spectrum are indicated with their corresponding mass and are clearly separated from each other. Each of the mass peaks contains contributions from several different isobars.

The multiplication by kinetic energy setting from Lohengrin is intended to cancel out the mass dependence, while retaining any electromagnetic effects in energy deposition (such as charge exchange) by a fragment, which have been introduced to the ϵ parameter through the division by the Q_{max} extracted directly from the pulse. Since the range is also proportional to A, the risetime parameter t_{10-90} was also adjusted by scaling it by FF A to normalize it in mass, producing the final quantity used in the analysis

$$\tau = \frac{t_{10-90}}{A}. \tag{3}$$

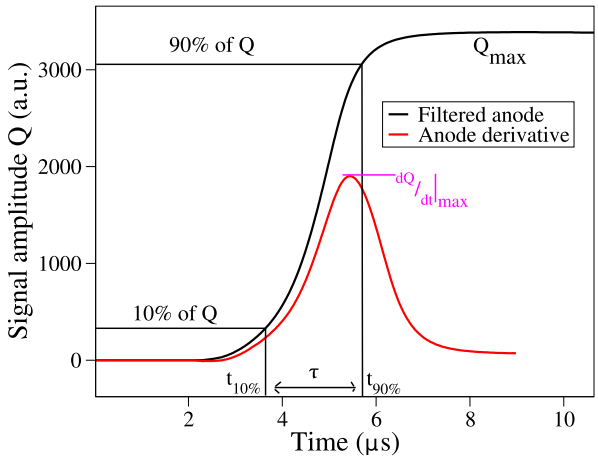

Fig. 4. A typical anode signal averaged over > 1000 FF shown with its derivative in red. The derivative has been shifted right and scaled for clarity. The parameters of interest corresponding to maximum energy, maximum energy loss, and 10% to 90% risetime are shown. (For interpretation of the references to colour in this figure legend, the reader is referred to the web version of this article.)

$A(\frac{v}{c})^2\epsilon$ and τ were plotted against velocities for a variety of FF masses and energies to extract velocity and Z-dependence of the two parameters. The parameters are shown in Fig. 5 where solid line fits show the resulting separation based on the given mass peaks' assigned average fragment proton number $\bar{Z}$. $\bar{Z}$ values were assigned based on charge yields from JEFF 3.1 [30] by performing a yield-weighted average for 7 atomic numbers with the highest yield for a given FF mass. Despite the contribution of several atomic numbers to $\bar{Z}$, the distribution of proton numbers contributing to any given mass selection is typically dominated by one single or at most two Z values (a typical yield-weighted standard deviation in $\bar{Z}$ is ≈0.2). Both data sets feature results extracted from the $\bar{Z} = 39$ fragments, which arrived at a similar A/q ratio with the heavy FF beam.[1] This allowed extending the data for the light fragments to lower velocities than typical. The $\bar{Z} = 39$ data have been a convenient test of the average proton number separation, since it is evident, that if the trends for this fragment mass were extrapolated to typical light fragment velocities, the line would pass where expected, i.e. between $\bar{Z} = 38$ and 40. The present experiment relied on high statistics provided by the intense FF beams at Lohengrin, while for many types of experiments it would be useful to assign Z based on individual FF ionization traces. Using the separation of the lines for different values of $\bar{Z}$ and assuming noise levels of 1% of Q_{max} in a trace, an estimated uncertainty δZ was calculated to be ≈4% for the both parameters, although τ estimate for δZ varied between 3.5% and 4.5% for different fragments and velocities, while the $A(\frac{v}{c})^2\epsilon$ estimate varied between 1% and 6%, and showed greater sensitivity to velocity. The fits were performed to the data to produce a functional form for future Z investigation using BDs. Previous efforts to fit the effective charge of FF during stopping have been considered as a possible component of the fitting form for energy loss, such as the Bethe–Bloch equation. A form for calculating equilibrium charge $\bar{q}$ been proposed by Betz et al. [32] and successfully applied to gas-filled recoil separators [33,34]. The dependence of $\bar{q}$ on v and Z of the FF takes the form

$$\bar{q} = Z\left[1 - C exp\left(-v/(v_0 Z^{\gamma})\right)\right], \tag{4}$$

where C is an experimentally-determined constant that depends on the gas and the FF, and γ is close to $2/3$. C has been measured for several gases by Betz et al. [32] and is typically slightly larger than 1, which means that as velocity goes to zero, equilibrium charge $\bar{q}$ does not approach zero. In the case of this work, where the FF fully stop in the gas (in contrast to a gas-filled separator) and become neutral, a power law dependence was chosen to fit the data. The fit has the form

$$\tau = a\bar{Z}^{\alpha}(v/c)^{\beta} \tag{5}$$

for fitting τ against velocity, and

$$A\left(\frac{v}{c}\right)^2\epsilon = a\bar{Z}^{\alpha+\gamma v/c}(v/c)^{\beta} \tag{6}$$

for the $A(\frac{v}{c})^2\epsilon$ fit against velocity. Here a, α, β and γ are fitted constants. The more complicated functional form shown in Eq. (6) was chosen, since fitting the $A(\frac{v}{c})^2\epsilon$ parameter with the simpler form of Eq. (5) resulted in reduced chi-squared of ≈9, motivating the introduction of the γ parameter. Conversely, functional form shown in Eq. (6) was also used to fit the τ parameter, however these more complicated fits showed no significant improvement.

Table 1
Fitting parameters extracted from fits of Eq. (5) to τ and of Eq. (6) to $A(\frac{v}{c})^2\epsilon$ obtained from the Lohengrin experiment with FiFI.

Fit parameter	τ (μs/amu)	$A(\frac{v}{c})^2\epsilon$ (amu/μs)
a	0.97 ± 0.04	154 ± 164
α	−0.83 ± 0.02	1.32 ± 0.08
β	0.29 ± 0.02	3.34 ± 0.31
γ	–	−14.3 ± 2.4

The fits to the two data sets are shown in Fig. 5 in solid lines: $A(\frac{v}{c})^2\epsilon$ results are on the left and τ results are on the right. The velocities were calculated based on Lohengrin settings for given FF energy and mass and corrected for energy loss in the gas window using SRIM toolkit [8]. While SRIM is known to calculate only an approximate value of energy loss in the relevant ion energy region, the change in velocity post-correction constituted ≲10%, and if SRIM result is accurate within 20% [35], then the correction introduces at most 2% uncertainty in the result, which was deemed acceptable. A further discussion of SRIM calculation reliability is given below. The fits to the chosen parameters as a function of corrected velocity are shown overlayed on the data in black solid lines. The fit to τ converged with reduced chi-squared $\chi^2_{red.} \approx 2$ and the fit to $A(\frac{v}{c})^2\epsilon$ converged with $\chi^2_{red.} \approx 4$. The final values of the fit parameters are summarized in Table 1. The scaling parameter a shows a large uncertainty (in excess of 100% for the $A(\frac{v}{c})^2\epsilon$ fit). This can be attributed to the fitting covariance in the parameters following the introduction of the γ degree of freedom, which is demonstrated by a small uncertainty in the scaling of τ, where γ parameter was not used.

The resulting values of the parameters for varying $\bar{Z}$ and the trends in their behaviour were compared to those extracted SRIM, since it is frequently used in research and industry to simulate the stopping of ions in matter. SRIM calculations for the stopping of ions at FF velocities are performed using the Lindhard–Scharff–Schiøtt (LSS) formalism [36]. SRIM simulations of energy loss and ranges for all the FF (except $\bar{Z} = 39$) used in the analysis of Lohengrin data were combined with electron drift velocity to obtain simulated τ and $A(\frac{v}{c})^2\epsilon$ parameters. Drift velocity was measured to be 3.119 ± 0.068 cm/μs for an ionization chamber with identical reduced field and fill gas settings to FiFI. The details of the process of extraction of electron drift velocities are presented in the work by S. Bennett et al. [37]. The plots of the resulting parameters against FF velocity are shown in dashed lines in Fig. 5 for $A(\frac{v}{c})^2\epsilon$ on the left and τ on the right. Both of the calculated parameters exhibit non-monotonic behaviour with $\bar{Z}$. SRIM is not an open-source toolkit, so the specific cause of discrepancies is hard to identify, however a likely reason lies in SRIM simulating fully ionized FF without accounting for possible initial population of electron states, which will strongly affect the subsequent energy loss through electron exchange, which is key to calculate stopping powers

[1] For thick uranium targets spending a long time in the high flux region part of the target material may diffuse into the Ti backing [31]. Ions released from deeper in will lose more energy and create a low energy tail to the natural fission fragment kinetic energy distribution.

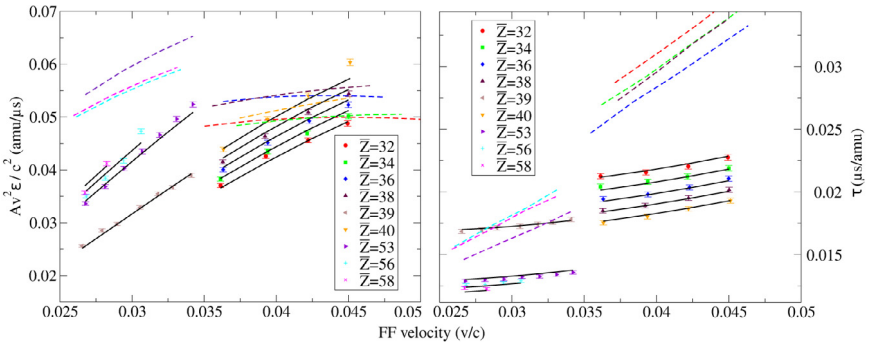

Fig. 5. Plots of $A(\frac{v}{c})^2\epsilon$ against FF velocity on the left and τ against velocity on the right. Lines corresponding to separate values of FF $\bar{Z}$ are easily distinguishable in both plots. There are two clusters present: one for heavy and one for light fragments. Functional fits to the parameters are in solid lines and results of a SRIM-2013 simulation for the same fragments are in dashed lines. See text for details.

in the FF velocity domain. It is clear from both parts of Fig. 5, that SRIM does not reproduce the parameters accurately. The trends in the risetimes appear to have the right overall increasing behaviour with velocity and consistently higher values for all the fragments. The $A(\frac{v}{c})^2\epsilon$ calculation does not reproduce the data trends at all. There, the data show an increase in $A(\frac{v}{c})^2\epsilon$ with increasing velocity for all fragments, but SRIM results only show such trends for the heavy fragments, while for light fragments the values of the energy-loss parameter are mostly constant. The values of both parameters calculated by SRIM disagree for heavy fragments, and there is disagreement between the data and the simulation for the risetime-like parameter for the light fragment group as well. The energy loss-like parameter values are similar for some of the light fragment group results and simulations at higher velocities. A closer agreement in this region is unsurprising, since more data would be available for this region as inputs for SRIM. The divergence between SRIM and the data for the risetime-like parameter in this region can be attributed to the difference in the definition of range, as SRIM calculates the range of FF as a depth in gas where FF is fully stopped, while the data only considers the 10% to 90% signal risetime. Furthermore, differences in the behaviour of the two measured parameters relative to SRIM need not show the same trends, since maximal energy loss will be computed in SRIM at a point, whereas range is a result of an integral. This difference in calculation may result in different predictions produced by SRIM relative to the available data.

The investigation by Filliatre *et al* [35] of SRIM performance in calculating ranges and energy loss in argon by ^{252}Cf fission fragments exhibited the opposite SRIM trends, whereby the simulated ranges were overestimated by 10%–20% and energy loss was underestimated by up to 23%. The work in Ref. [35] relies on measurements of range performed by M. Pickering and J.M. Alexander [38] and energy loss measurements by M. Forte et al. [39]. The comparison between the measurements of energy loss presented here and in the work by Forte et al. is difficult due to different method of extracting energy loss, since it is averaged over the FF range in Ref. [39], whereas the current work uses maximal energy loss.

The range measurements in Ref. [38] used a ^{252}Cf source, fission fragments from which travelled into a volume of fill gas through a collimator and a nickel window. The fill gases considered in that work are hydrogen, helium, neon, and argon. The stopped fragments were swept by an electric field applied perpendicularly to the fragment track, and deposited onto an aluminium foil. The foil was then cut into strips and gamma-ray spectroscopic techniques were applied using a Ge(Li) detector to identify the species of β-decayed fission products, while the position of the strip was used to measure range. The differences in fill gases between the current work and Ref. [38] mean that the absolute ranges will be different, and differences in proton numbers due to β decay mean that the comparison of the behaviour of different charge states cannot be made. Furthermore, Pickering and Alexander do not present the results for any of the same mass nuclei as this work except $A = 97$, which in the case of this work was measured at uncharacteristically low energies due to scattering. Nonetheless, a general trend of ranges with mass can be considered.

Reduced ranges (range multiplied by fill gas density) have been deduced for a gas density of 0.233 ± 0.001 mg/cm^3, which was found based on the ideal gas law and assigned an uncertainty determined by variations in gas pressure observed during the campaign (≈0.3 mbar). Reduced ranges were calculated based on the 10% to 90% risetime of the filtered and averaged anode signals multiplied by the electron drift velocity, which was the dominant contributor to the reduced range uncertainty. A list of ranges and maximal energy losses measured in this work is given in Table 2 (both sets of values are scaled by gas density).

A plot of reduced ranges against nuclear mass for the current data and the data of Pickering and Alexander is presented in Fig. 6. The reduced range values are broadly of the same magnitude as the results in Ref. [38], however the results presented by Pickering and Alexander show a more pronounced decrease with increasing fission product mass. The data presented in this work appear to have ranges that reduce only marginally with increasing mass within the uncertainties. The current data for reduced ranges rely on the 10% to 90% anode risetime for calculating ranges, whereas the data of Pickering and Alexander is based on the final position of the fission fragment before being swept by the electric field onto the foil. This difference in measurement technique may mean that for a full comparison of the values, the current data would need to be scaled. The overall trend of both the current data and the results by Pickering and Alexander is decrease in range with increase in mass, which is expected, since the more massive FF travel at lower energies and also typically have higher atomic number, which will cause them to have lower range in gas. SRIM confirms the overall ordering of the range dependence on fill gas, although it fails to reproduce the values of either Ref. [38] or the current work. Indeed as suggested by the work of Filiatre et al. SRIM does underestimate the ranges of the work of Pickering and Alexander, and as indicated in Fig. 5 the ranges of the current data set are overestimated, however this difference can be accounted for with some scaling parameter that would compensate for different methods for interpreting the range.

FF ranges deduced from the risetime parameter were compared with ranges calculated by integrating the differential energy loss. There was an overall agreement to ≈20% on average between the risetime calculations and the energy loss integral, and the difference was the greatest (≈30%) for the lightest FF ($\bar{Z}$=32) and for the three heavy fragments. The disagreement of the two calculations suggests that the form of the fit cannot be safely extrapolated to low FF velocities at better than 20% accuracy and is only applicable at the narrow velocity range used for fitting.

4. Conclusion

Measurements using the FiFI spectrometer have been performed at the Lohengrin separator at ILL in order to characterize the response of

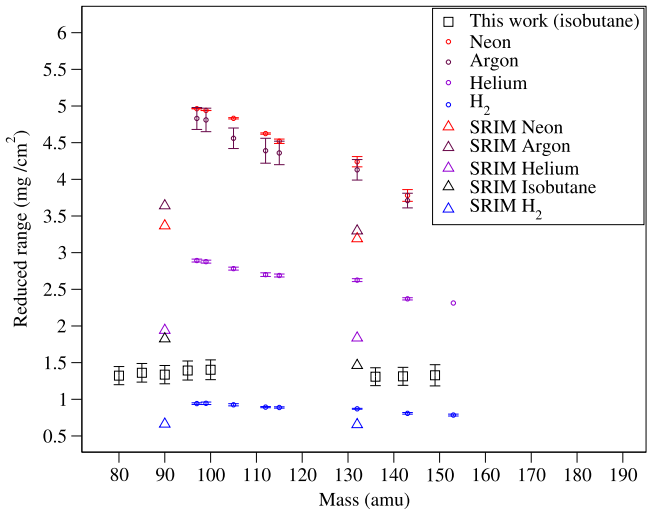

Fig. 6. Reduced ranges presented in this work compared to measurements by Pickering and Alexander [38] for several fill gases. The current work relied on isobutane as fill gas, while the work in Ref. [38] presented measurements for neon (magenta), argon (red), helium (purple) and hydrogen (blue). The data from this work shown in the figure above correspond to Lohengrin settings with the most likely energies for a given mass as determined by count rate and have their energies highlighted in red in Table 2. (For interpretation of the references to colour in this figure legend, the reader is referred to the web version of this article.)

BDs to ^{235}U fission fragments in varying charge states. Fragments were selected based on their mass, kinetic energy and charge to produce beams of known composition. Ionization signal traces were collected and filtered using calibrated digital filters. Two parameters were extracted from the filtered anode signals gated in mass and energy. The energy loss-like and the risetime-like parameters, $A(\frac{v}{c})^2\epsilon$ and τ, were plotted against fragment velocity to examine their dependence on charge in analogy to the Bethe–Bloch formula. The resulting plots show these parameters exhibit a strong dependence on Z. Fission fragment ranges in isobutane were also calculated based on anode signal risetimes and are presented in Table 2.

Similar plots were produced by applying the energy loss-like and the risetime-like parameters to simulated results from SRIM-2013. The simulation results were found to disagree with the experimental work both quantitatively and in general trends with increasing velocity for the energy loss-like parameter. The experimental trends are similar in SRIM and the experiment for the risetime-like parameter, however there is still a considerable quantitative disagreement. Moreover, for certain fragment charge ranges SRIM exhibits non-monotonic behaviour unlike the experimental data.

The calibration fits for extracting $\bar{Z}$ are currently being investigated using ^{252}Cf in order to assess their performance with a fission fragment source without pre-selected mass, energy and effective charge. The technique will be applied to the measurements by extracting the FF mass from the energy and velocity measurements, calculating the energy loss and risetime parameters, and mapping the calibration functions onto the distributions of the parameters as a function of velocity in order to assign a likely Z-value for a given mass.

5. Supplementary materials

The raw data are available via Ref. [40].

Declaration of competing interest

The authors declare that they have no known competing financial interests or personal relationships that could have appeared to influence the work reported in this paper.

Table 2
Reduced ranges in mg/cm^2 for fission fragments listed for varying A and E Lohengrin settings. The ranges are grouped by calculated $\bar{Z}$ values and ordered by increasing energy. The energy settings chosen for comparison with [38] based on count rate are highlighted in red.

$\bar{Z}$	A (amu)	E (MeV)	Reduced range (mg/cm^2)	Reduced maximal energy loss (MeV cm^2/mg)
32	80	53	1.24 ± 0.13	23.3 ± 1.2
32	80	62	1.25 ± 0.13	21.8 ± 1.3
32	80	71	1.28 ± 0.12	18.4 ± 1.4
32	80	80	1.32 ± 0.12	16.1 ± 1.5
34	85	56	1.26 ± 0.12	23.6 ± 1.2
34	85	66	1.29 ± 0.12	21.2 ± 1.4
34	85	75	1.31 ± 0.12	18.5 ± 1.4
34	85	85	1.35 ± 0.13	15.9 ± 1.5
34	85	94	1.36 ± 0.13	8.7 ± 1.6
36	90	60	1.25 ± 0.12	23.7 ± 1.3
36	90	70	1.28 ± 0.12	21.4 ± 1.4
36	90	80	1.30 ± 0.12	18.9 ± 1.5
36	90	90	1.34 ± 0.12	16.3 ± 1.6
38	95	63	1.28 ± 0.12	24.4 ± 1.3
38	95	73	1.31 ± 0.12	21.9 ± 1.4
38	95	84	1.35 ± 0.13	19.3 ± 1.6
38	95	95	1.39 ± 0.13	16.7 ± 1.6
39	97	35.7	1.19 ± 0.11	33.5 ± 1.0
39	97	39.2	1.20 ± 0.11	33.9 ± 1.1
39	97	42	1.21 ± 0.11	31.6 ± 1.1
39	97	46.4	1.2 ± 0.11	31.0 ± 1.2
39	97	49.9	1.23 ± 0.11	30.6 ± 1.2
39	97	53	1.24 ± 0.12	28.6 ± 1.2
39	97	57	1.25 ± 0.12	27.5 ± 1.3
40	100	66	1.27 ± 0.12	26.2 ± 1.4
40	100	77	1.31 ± 0.12	23.8 ± 1.5
40	100	88	1.35 ± 0.13	21.0 ± 1.6
40	100	100	1.40 ± 0.13	19.9 ± 1.8
53	136	50	1.27 ± 0.12	40.1 ± 1.3
53	136	55	1.28 ± 0.12	39.2 ± 1.3
53	136	60	1.29 ± 0.12	38.8 ± 1.4
53	136	65	1.31 ± 0.12	38.0 ± 1.5
53	136	70	1.31 ± 0.12	37.2 ± 1.6
53	136	75	1.32 ± 0.12	36.3 ± 1.6
53	136	80	1.34 ± 0.13	35.1 ± 1.7
56	142	52	1.29 ± 0.12	41.7 ± 1.3
56	142	57	1.30 ± 0.12	41.2 ± 1.4
56	142	62	1.31 ± 0.12	40.5 ± 1.5
56	142	67	1.33 ± 0.13	44.4 ± 1.6
58	149	54	1.34 ± 0.12	41.9 ± 1.3
58	149	60	1.33 ± 0.14	44.7 ± 1.5

CRediT authorship contribution statement

N.V. Sosnin: Data curation, Formal analysis, Investigation, Methodology, Ssoftware, Visualization, Writing - original draft, Writing - review & editing. **A.G. Smith:** Data curation, Formal analysis, Funding acquisition, Investigation, Methodology, Project administration, Resources, Software, Supervision, Writing - review & editing. **T. Wright:** Formal analysis, Funding acquisition, Investigation, Methodology, Project administration, Supervision, Writing - review & editing. **U. Köster:** Formal analysis, Funding acquisition, Investigation, Methodology, Project administration, Resources, Supervision, Writing - review & editing. **A. Blanc:** Data curation, Formal analysis, Investigation, Resources, Software, Supervision. **B.S. Nara Singh:** Investigation, Writing - review & editing. **R.L. Kennedy-Reid:** Formal analysis, Writing review & editing. **P.J. Davies:** Software, Writing - review & editing.

Acknowledgements

The authors would like to acknowledge STFC, UK (grant ST/N00244X/1) and EPSRC, UK (grant EP/N00700X/1) for financing the project.

References

[1] H. Geiger, E. Marsden, On a diffuse reflection of the α particles, Proc. R. Soc. A82 (1909) 495–500.
[2] C.R. Gruhn, et al., Bragg curve spectroscopy, Nucl. Instrum. Methods 196 (1982) 33–40.
[3] J.M. Asselineau, et al., Performance of a bragg curve detector for heavy ion identification, Nucl. Instrum. Methods 204 (1982) 109–115.
[4] A. Oed, P. Geltenbort, F. Gönnenwein, A new method to identify nuclear charges of fission fragments, Nucl. Instrum. Methods 205 (1983) 451–453.
[5] W. Neubert, Bragg curve spectroscopy of fission fragments by using parallel plate avalanche counters, Nucl. Instrum. Methods A 237 (1985) 535–542.
[6] E. Pellereau, et al., Accurate isotopic fission yields of electromagnetically-induced fission of ^{238}U measured in inverse kinematics at relativistic energies, Phys. Rev. C 95 (2017) 054603.
[7] N. Bohr, Scattering and stopping of fission fragments, Phys. Rev. 58 (1940) 654–655.
[8] J.F. Ziegler, M.D. Ziegler, J.P. Biersack, SRIM - The stopping and range of ions in matter (2010), Nucl. Instrum. Methods B 268 (2010) 1818–1823.
[9] W. Reisdorf, et al., Fission fragment K X-ray emission and nuclear charge distribution for thermal neutron fission of ^{233}U, ^{235}U, ^{239}Pu and spontaneous fission of ^{252}Cf, Nuclear Phys. A 177 (1971) 337–378.
[10] J.N. Wilson, et al., Anomalies in the charge yields of fission fragments from the ^{238}U(n,f) reaction, Phys. Rev. Lett. 118 (2017) 222501.
[11] T. Materna, et al., Studies of fission fragment de-excitation by gamma-ray spectroscopy with the EXILL experiment, EPJ Web Conf. 146 (2017) 04041.
[12] D.C. Biswas, M.N. Rao, R.K. Choudhury, Specific energy-loss behaviour of fission fragments along their range in P-10 gas, Nucl. Instrum. Methods B 53 (1991) 251–254.
[13] D. Ramos, et al., Isotopic fission-fragment distributions of ^{238}U, ^{239}Np, ^{240}Pu, ^{244}Cm, and ^{250}Cf produced through inelastic scattering, transfer, and fusion reactions in inverse kinematics, Phys. Rev. C 97 (2018) 054612.
[14] A. Singh, et al., Performance study of an integrated ΔE-E silicon detector telescope using the Lohengrin fission fragment separator at ILL, Grenoble, IEEE Trans. Nucl. Sci. 62 (2015) 264–271.
[15] J.P. Bocquet, R. Brissot, H.R. Faust, A large ionization chamber for fission fragment nuclear charge identification at the lohengrin spectrometer, Nucl. Instrum. Methods A 267 (1988) 466–472.
[16] S. Dubey, et al., Application of calorimetric low-temperature detectors for th einvestigation of Z-yield distributions of fission fragments, J. Low Temp. Phys. 193 (2018) 1257–1262.
[17] H. Paşca, et al., Toward an understanding of the anomaly in charge yield of Mo and Sn fragments in the fission reaction ^{238}U(n,f), Phys. Rev. C 98 (2018) 014624.
[18] N.E. Stauff, T.K. Kim, T.A. Taiwo, Vairations in nuclear waste management performance of various fuel-cycle options, J. Nucl. Sci. Technol. 52 (2015) 1058–1073.
[19] N. Shinohara, et al., Measurements of fission product yields from neutron-induced fission of americium-241, J. Nucl. Sci. Technol. 36 (1999) 232–241.
[20] A.A. Sonzogni, E.A. McCutchan, A.C. Hayes, Dissecting reactor antineutrino flux calculations, Phys. Rev. Lett. 119 (2017) 112501.
[21] S.D. Clarke, et al., Measurement of the energy and multiplicity distributions of neutrons from the photofission of ^{235}U, Phys. Rev. C 95 (2015) 064612.
[22] E. Blain, et al., Measurement of prompt fission neutron spectrum for spontaneous fission of ^{252}Cf using γ multiplicity tagging, Phys. Rev. C 95 (2017) 064615.
[23] L. Qi, et al., Statistical study of the prompt-fission γ-ray spectrum for ^{238}U(n,f) in the fast neutron region, Phys. Rev. C 98 (2018) 014612.
[24] L. Gaudefroy, et al., A twin-frisch grid ionization chamber as a selective detector for the delayed gamma-spectroscopy of fission fragments, Nucl. Instrum. Methods A 855 (2017) 133–139.
[25] E. Murray, et al., Measurements of gamma energy distributions and multiplicities using STEFF, Nucl. Data Sheets 119 (2014) 217–220.
[26] Hamamatsu Photonics, MCP (Microchannel Plate) and MCP Assembly, 2016.
[27] P. Armbruster, et al., The recoil separator lohengrin: performance and special features for experiments, Nucl. Instrum. Methods 139 (1976) 213–222.
[28] V.T. Jordanov, G.F. Knoll, Digital synthesis of pulse shapes in real time for high resolution radiation spectroscopy, Nucl. Instrum. Methods A 345 (1994) 337–345.
[29] A. Göök, et al., Application of the Shockley-Ramo theorem on the grid ineffi-ciency of frisch grid ionization chambers, Nucl. Instrum. Methods A 664 (2012) 289–293.
[30] A. Koning, et al., The JEFF-3.1 Nuclear Data Library, 2006.
[31] U. Köster, et al., Application of calorimetric low-temperature detectors for the investigation of Z-yield distributions of fission fragments, Nucl. Instrum. Methods A 613 (2010) 363–370.
[32] H.-D. Betz, et al., The average charge of stripped heavy ions, Phys. Lett. 22 (1966) 643–644.
[33] H. Lawin, et al., The Jülich On-line Separator for Fission Products "JOSEF", Nucl. Instrum. Methods 137 (1976) 103–117.
[34] A. Chebboubi, et al., Development of a gas filled magnet spectrometer within the FIPPS project, Nucl. Instrum. Methods B 376 (2016) 120–124.
[35] P. Filliatre, C. Jammes, B. Geslot, Stopping power of fission fragments of ^{252}Cf in argon: a comparison between experiments and simulation with the SRIM code, Nucl. Instrum. Methods A 618 (2010) 294–297.
[36] J. Lindhard, M. Scharff, H.E. Schiøtt, On the properties of a gas of charged particles, Mat.-Fys. Medd. Dan. Vidensk. Selsk. 53 (1963).
[37] S.A. Bennett, et al., Development of a novel segmented anode Frisch-grid ionisation chamber for fission measurements, Nucl. Instrum. Methods A 951 (2019) 162846.
[38] M. Pickering, J.M. Alexander, Range measurements of fission products I. comparison with stopping theory, Phys. Rev. C 6 (1972) 332–343.
[39] M. Forte, et al., Experimental study on the energy loss in argon of ^{252}Cf fission fragments, Phys. Rev. B 14 (1976) 956–968.
[40] N.V. Sosnin, et al., Digital Sub-Bragg-Peak Spectroscopy at Lohengrin, 2016, http://dx.doi.org/10.5291/ILL-DATA.3-01-648.